Ultrafast manipulation of magnetic anisotropy in a uniaxial intermetallic heterostructure TbCo 2 /FeCo

Sergei Ovcharenko, Mikhail Gaponov, Alexey Klimov, Nicolas Tiercelin, Philippe Pernod, Elena Mishina, Alexander Sigov, Vladimir L. Preobrazhensky

Ultrafast manipulation of magnetic anisotropy in a uniaxial intermetallic heterostructure $TbCo_2$/FeCo

Sergei Ovcharenko[1], Mikhail Gaponov[1], Alexey Klimov[1], Nicolas Tiercelin[2], Philippe Pernod[2], Elena Mishina[1], Alexander Sigov[1] and Vladimir Preobrazhensky[3]

1 MIREA—Russian Technological University, Moscow 119454, Russia
2 Univ. Lille, CNRS, Centrale Lille, Univ. Polytechnique Hauts-de-France, UMR 8520-IEMN, 59000 Lille, France
3 Prokhorov General Physics Institute of RAS, Moscow 119991, Russia

Abstract
We study experimentally and theoretically the dynamics of spin relaxation motion excited by a femtosecond pulse in the $TbCo_2$/FeCo multilayer structures with different ratios of $TbCo_2$ to FeCo thicknesses $r_d = d_{TbCo2} / d_{FeCo}$. The main attribute of the structure is in-plane magnetic anisotropy that is artificially induced during sputtering under a DC magnetic field. The optical pump-probe method revealed strongly damped high-frequency oscillations of the dynamical Kerr rotation angle, followed by its slow relaxation to the initial state. Modeling experimental results using the Landau–Lifshitz-Gilbert (LLG) equation showed that the observed entire dynamics is due to destruction and restoration of magnetic anisotropy rather than to demagnetization. For the pumping fluence of 7 mJ cm−2, the maximal photo-induced disruption of the anisotropy field is about 14% for the sample with rd = 1 and decreases when rd increases. The anisotropy relaxation is a three-stage process: the ultrafast one occurs within several picoseconds, and the slow one occurs on a nanosecond time scale. The Gilbert damping in the multilayers is found to be one order of magnitude higher than that in the constituent monolayers.

Keywords: ultrafast magnetization dynamics, magnetic anisotropy, spintronics, pump-probe, Landau–Lifschitz–Gilbert equation

1. Introduction

The manipulation of the spin system parameters in magnetic structures underlies the principle of modern spintronic devices. The operation rate of devices based on switching of magnetic states is determined by the precession frequency and relaxation time of the spin system. These two parameters can be selected appropriately depending on the type of device. In particular, the elements of magnetic random-access memory (MRAM) and spin valves require high damping (short relaxation time) of the precession [1, 2]. On the contrary, spin-wave logic devices [3, 4] and spin-torque nano-oscillators [5, 6] require low damping. The limit for operation rate of all spintronic devices is ferromagnetic resonance (FMR) frequency [7].

To achieve a switching frequency that meets modern requirements, the relaxation times must be so short that traditional methods of measuring based upon FMR have become inapplicable due to a huge broadening of the resonance line. In this case, the magneto-optical technology using femtosecond laser radiation provides adequate methods for recording and analyzing ultrafast spin processes [8, 9]. Moreover, advances in ultrafast control of magnetic media with femtosecond laser pulses has begun a new era of opto-magnetism, allowing the development of new devices that operate at high frequency and low power consumption, which cannot be achieved with other techniques.

Optical spin manipulation is most often implemented through ultrafast demagnetization [10–13]. At the same time, femtosecond radiation has a wide range of mechanisms for affecting the spin system. In particular, in a number of systems, the result of optical impact is ultrafast disruption of magnetic anisotropy: in substituted yttrium iron garnet films [14, 15], thin iron films [16], galfenol films [17].

Among the systems where magnetic anisotropy plays a crucial role for the device functionality are intermetallic multilayers. The most studied ferromagnetic (FM)/nonmagnetic (NM) multilayers with perpendicular anisotropy are used for MRAM with ultrafast recording [18]. The FM/NM and FM/FM

structures with in-plane anisotropy are used as spintronic THz emitters [19,20]. The FM/FM structures, such as $TbCo_2$/FeCo multilayers with in-plane anisotropy are very prospective for creation of magnetoelectric random access memory (MELRAM) with ultra-low energy consumption about a few attojoule per bit [21]. The principle of operation of such devices is based on spin reorientation transitions (SRT) in the magnetic constituent, induced by short strain pulses generated by piezoelectric constituent elastically coupled with the structure. The switching rate between magnetic states in the MELRAM cells was estimated as fractions of a nanosecond. However, the limit of the operation rate determined by dynamic behavior of the spin system under ultrafast excitation is still an open question for these types of multilayers.

The aim of this work is to reveal the general patterns of the spin dynamics of $TbCo_2$/FeCo multilayers under ultrafast optical impact. For this, the samples with different ratios of thicknesses of $TbCo_2$ and FeCo layers and different total number of the bilayers were studied. Experimentally, dynamics of the Kerr rotation angle was studied by the optical pump-probe method. Modeling of the experimental results using the Landau–Lifshitz–Gilbert (LLG) equation shows that the observed dynamics occurs due to destruction and restoration of magnetic anisotropy rather than due to demagnetization.

2. Materials and methods

A series of N×[$TbCo_2$/FeCo]/Ru multilayer structures with an interlayer exchange are studied. The samples differ in the number of double layers N, and in the thicknesses of $TbCo_2$ and FeCo layers. The structures were deposited on top of SiO2 substrate and an Ru cap layer is used to prevent oxidation. Deposition was performed by RF sputtering in a constant magnetic field used to induce uniaxial magnetic anisotropy in the plane of the structure [22]. A change in layer thickness leads to a change in the magnitude of the induced magnetic anisotropy [23, 24]. For reference, FeCo and $TbCo_2$ layers were also fabricated. The thicknesses of the layers in each sample were controlled by the sputtering operating mode. Parameters of the samples are given in table 1.

The magnetic properties of the samples were investigated using a vibration magnetometer. For these measurements, an external magnetic field was applied in the plane of the film either along the direction of the easy magnetization axis (in the following ‘easy axis’ configuration) or at 90 degrees to it (in the following ‘hard axis’ configuration). Magnetization hysteresis loops are shown in figure 1.

Interestingly, ordering in $TbCo_2$/FeCo structures is ferri-magnetic, while both $TbCo_2$ and FeCo at room temperature reveal FM order [25, 26]. The magnetizations of the $TbCo_2$ and FeCo layers are opposite. In all studied samples, the compensation point is below room temperature, and the resulting magnetization of the structure is directed along the magnetization of FeCo. The exchange coupling of the layers maintains the antiparallel orientation of the magnetizations, and the static and dynamic behavior of the system at not too strong magnetic fields and practically attainable frequencies is similar to the FM coupling, which is confirmed by the magnetization curves shown in figure 1. The description of the dynamics of such systems in the FM model is typical for ferrites.

The shape of the loops confirms unambiguously the in-plane uniaxial anisotropy of the structures. The values of saturation magnetization Ms and anisotropy field H_A obtained from the loops are given in table 1.

For the easy axis direction of magnetization, the loops are rectangular, and coercivity of A, B, C samples is small within the error bar. The highest saturation magnetization Ms is observed for the sample C, and lowest Ms is observed for the sample D, the difference is about 2.5 times. The lowest anisotropy field is obtained for the sample A, about twice higher HA is observed for the samples B and C, while in the sample D the anisotropy field is much higher. Both $TbCo_2$ and FeCo reference films have anisotropy fields lower than multilayer structures. The magnetization of FeCo film is the highest one among all the samples studied, while the magnetization of $TbCo_2$ film is comparable to those of multilayer structures.

The optically induced magnetization dynamics in the $TbCo_2$/FeCo structures were studied by the pump-probe technique. The geometry of the experiment is shown in figure 2. The z axis of the laboratory frame is directed along the sample normal, and the x axis was chosen along the easy magnetization axis. An external magnetic field H was applied during the measurement at an angle of 45° to the plane of the sample, with a projection onto the easy axis of magnetization. The laser pulses with duration of 35 fs, central wavelength of 800 nm and repetition rate of 3 kHz were split into pump and probe channels in a 10 to 1 ratio (laser system includes a TiF-20F femtosecond Ti: Sapphire laser and a regenerative amplifier designed by ‘Avesta-project’, Russia). The pump-probe temporal delay t is controlled by a

delay line in the pump optical path. The P-polarized pump and probe beams were focused onto the sample with fluence of about 7 and 0.7mJ cm^{-2}, respectively. The angle of incidence for the probe beam was 45°, and for the pump pulse it was 20°. All measurements were performed at room temperature.

Table 1. The samples structures and static magnetic parameters.

Sample	Structure	rd	Ms, kemu cm−3	HA, kOe
A	FeCo 2 nm/2×[$TbCo_2$ 4 nm /FeCo 4 nm]/ $TbCo_2$ 4 nm/FeCo 2 nm/Ru 4 nm	1	0.63	1.1
B	FeCo 2 nm/2×[$TbCo_2$ 4.8 nm/FeCo 4 nm]/TbCo2 4.8 nm/FeCo 2 nm/Ru 4 nm	1.2	0.48	2
C	FeCo 4 nm/6×[$TbCo_2$ 4.2 nm/FeCo 4 nm]/Ru 4 nm	1.05	0.8	1.9
D	FeCo 1 nm/14×[$TbCo_2$ 2.4 nm/FeCo 1.5 nm]/FeCo 1 nm	1.6	0.48	8
FeCo layer	10 nm	n/a	1.5	0.1
TbCo2 layer	10 nm	n/a	0.65	0.2

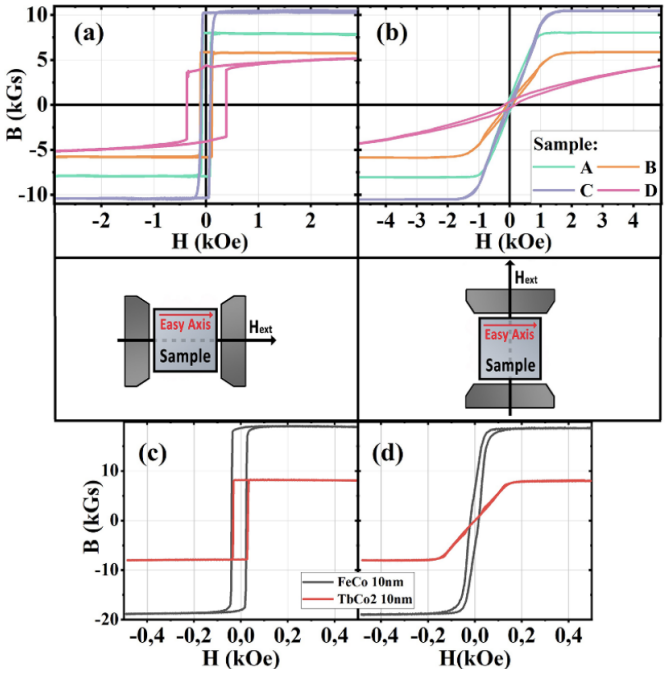

Figure 1. Magnetization hysteresis loops of the samples of multilayer structures and reference thin films in the 'easy axis' (a), (c) and 'hard axis' (b), (d) configurations of magnetic anisotropy. The insets show the magnetization measurements geometry.

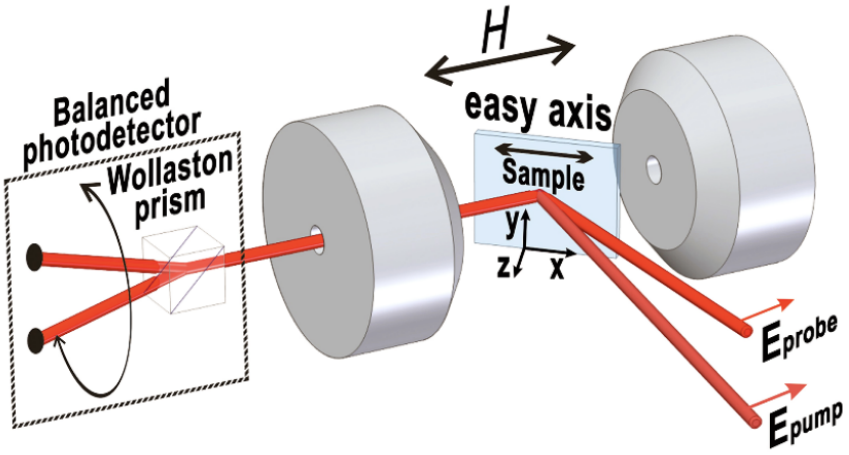

Figure 2. The pump-probe experimental geometry.

The detection of magnetization dynamics in this geometry is based on the time-resolved magneto-optical Kerr effect (TR-MOKE) [16, 27, 28]. The geometry used allowed detecting the simultaneous dynamics of the polar and longitudinal Kerr effects (TR-PMOKE and TR-LMOKE). The polarization rotation angles ΔθK(t, H) for TR-LMOKE and TR-PMOKE are proportional to in-plane and out-of-plane components of magnetization Mx and Mz, respectively.

In the experiment, the temporal dependences of the photoinduced Kerr polarization rotation angle ΔθK(t, H) and the intensity of the reflected probe beam ΔR(t) were detected simultaneously by an optical bridge, consisting of the Wollaston prism and the balanced photodetector, at the external magnetic field with different magnitudes. The data processing details are given in the appendix. Within the experimental geometry, contribution of two effects into the total Kerr effect as $\Delta\theta_K(t,H) = \Delta\theta_{\text{TR-LMOKE}}(t,H) - k \cdot \Delta\theta_{\text{TR-PMOKE}}(t,H)$ can be determined. The fitted data yielded k = 0.7 for all the samples.

3. Results and discussion

The results of the photoinduced polarization rotation angle dynamics ΔθK(t, H) of all samples studied are shown in figure 3. In the pure FeCo and $TbCo_2$ films, strong oscillations with low damping were observed. On the contrary, in all $TbCo_2$/FeCo multilayers, oscillations were strongly damped and became undistinguished after two (samples A,C) or even one period (samples B,D). An estimate of the magnetic moment precession frequency upon destruction of the magnetic anisotropy by an optical pulse gives the value of about 20 GHz for the maximum value of the external magnetic field, used in the experiment. The numerical model of the photoinduced spin dynamics is based on the LLG equation in angular representation:

$$\begin{aligned} \frac{\partial\phi}{\partial t} &= \frac{\gamma M_s}{\Delta}\left[\sin\theta\frac{\partial F}{\partial\theta} - \alpha\frac{\partial F}{\partial\phi}\right] \\ \frac{\partial\theta}{\partial t} &= \frac{\gamma M_s}{\Delta}\left[\sin\theta\frac{\partial F}{\partial\phi} - \alpha\sin^2\theta\frac{\partial F}{\partial\theta}\right] \end{aligned} \quad (1)$$

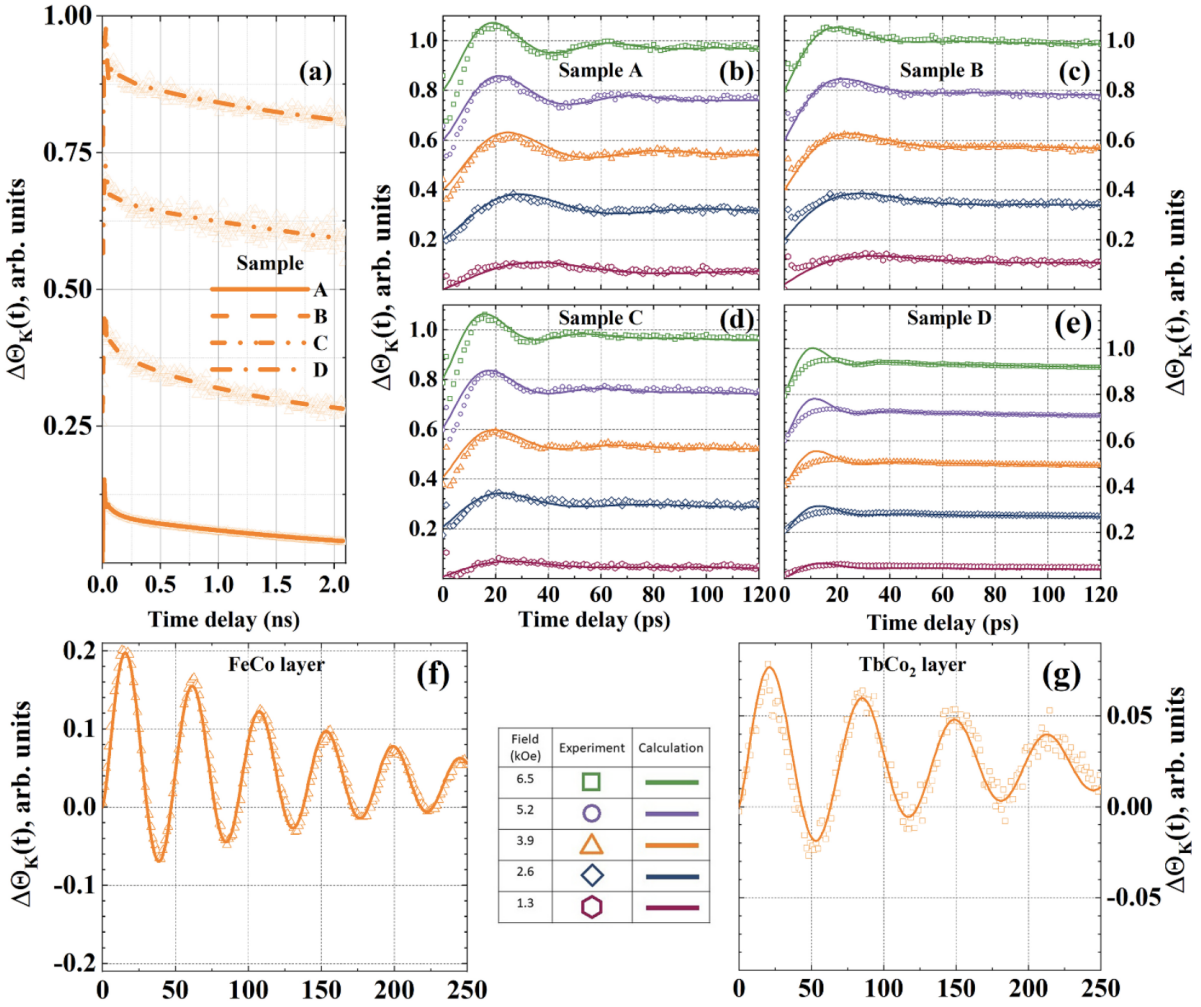

Figure 3. Results of experiments (points) and modeling (lines) of photoinduced magnetization dynamics for various values of the external magnetic field in multilayer structures (a)–(e) and in reference layers (f), (g). The graphs (a)–(e) are presented with an offset along the OY axis. Colors in all graphs corresponds to the magnetic field values given in the inset.

In which, the angular variables φ and θ determine projections of the magnetic moment Mx = Ms sin θ cos φ, My = Ms sin θ sin φ, Mz = Ms cos θ; F is the free energy density, γ is gyromagnetic ratio, Δ = Ms^2 (1 + α^2) $\sin^2$ θ and α is the Gilbert spin relaxation parameter. Ultrafast disruption of magnetic anisotropy in a thin cobalt film as a result of photoinduced excitation was first shown in [29]. The same effect was assumed for intermetallic heterostructure in [30]. In the framework of phenomenological theory used in micromagnetism, and assuming the ultrafast disruption of magnetic anisotropy, we can write down the FM free energy density F. It consists of four terms: magnetic anisotropy energy with the time dependent anisotropy field $H_A(t)$, energy of magnetic moment M interactions with external field (Zeeman energy), determined by Hx and Hy, and demagnetizing field (magnetostatic energy) determined by Mz projection:

$$F = -\frac{1}{2}M_s H_A(t)\sin^2\theta\cos^2\phi - H_x M_s \sin\theta\cos\phi - H_y M_s \sin\theta\sin\phi + 2\pi {M_s}^2 \cos^2\theta. \quad (2)$$

To describe the process of anisotropy relaxation after optical impact, we used the three–exponential decay time dependence of the anisotropy field on time:

$$H_A(t) = H_A\left(1 - A_{th}e^{-t/\tau_{th}} - A_1 e^{-t/\tau_1} - A_2 e^{-t/\tau_2}\right), \quad (3)$$

where τ_{th} is the thermalization time, that is the time of the initial partial recovery of spins, electrons and lattice to equilibrium with each other and usually estimates for magnetic metals as 1–4 ps [31–33]. The fitting procedure was as follows. First of all, we estimated the largest time constant τ_2 from the long-time-scale dependences. The estimation gives the values of 1 ÷ 4 ns. For the thermalization time we took the average value obtained from the fit of initial part of the relaxation dependences τ_{th} = 2.4ps, which gives us the amplitude A_{th} = 1%. After that, for each sample, a complete simultaneous fit using equations 1-3 was performed with 3 fitting parameters: A_1, τ_2 and A_2. While introducing the additional term $A_1 e^{-t/\tau 1}$, we refer to the latest work [34] where the experimental timescale was divided into two time ranges corresponding to the range of the transient changes of the magnetic parameters following the excitation (<0.5 ns), and the range of parameters corresponding to the cooled film (>0.5 ns). Parameters A_{th}, A_1 and A_2 are the amplitude of the anisotropy disruption. We consider the sum of these amplitudes $A_{th} + A_1 + A_2$, expressed as a percentage, as a fraction of the total anisotropy disrupted by optical excitation.

The values of saturation magnetization Ms and the anisotropy field H_A were obtained from magnetometry (see table 1) and inserted into equations (2) and (3). For each sample, the simultaneous fit was performed over five experimental dependences for different values of external magnetic field using equations (1)–(3). The calculated parameters were the Gilbert damping α, time constants and amplitudes of the two stages of the anisotropy recovery. The results are shown in figure 4.

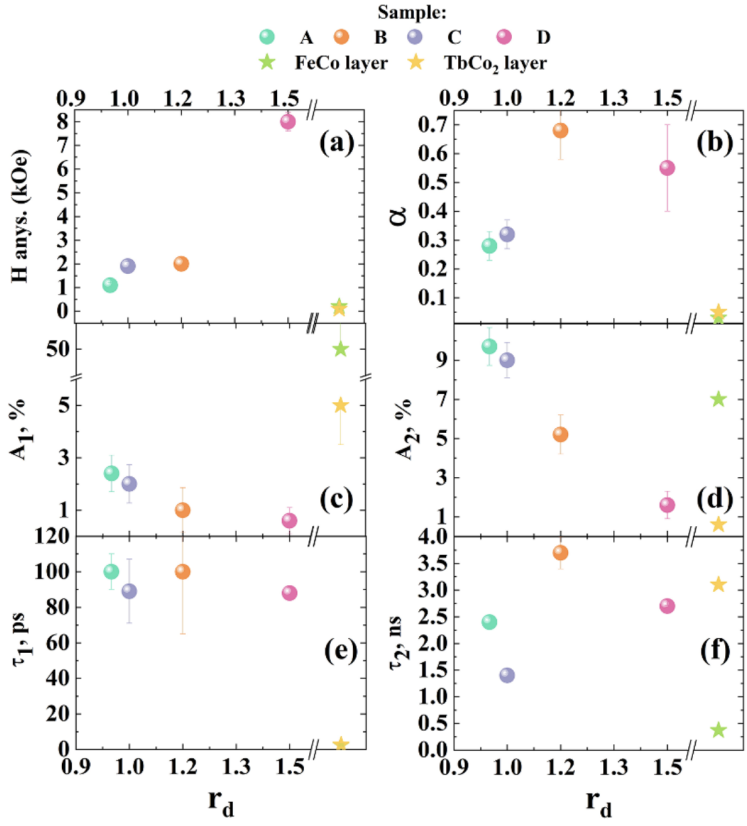

Figure 4. Dependences of the anisotropy field HA (a), Gilbert damping parameter α (b), anisotropy disruption amplitudes A_1(c), A_2(d) and thermal relaxation time constants τ_1 (e) and τ_2 (f) on the ratio $r_d = d_{TbCo2}/d_{FeCo}$. The calculation parameters for pure $TbCo_2$ and FeCo layers are given for reference as stars. For all samples τ_{th} = 2.4 ps.

For multilayers, magnetic anisotropy is determined by the thickness ratio $r_d = d_{TbCo2}/d_{FeCo}$ [23, 24] and increases with r_d increase in the range of rd = 1.4–1.5 (figure 4(a)). The dependence of the anisotropy $H_A(d_r)$ is explained by the fact that its value is determined by the rare earth component. Therefore, the higher the ratio $rd = d_{TbCo2}/d_{FeCo}$, the greater the amount of Tb and the anisotropy. The suppression of

the anisotropy expressed as the amplitudes $A_{1,2}$ is weaker, the larger its value. Time constants behaves differently. $\tau_1(d_r)$ = 90 ps and is a constant within the error bar for all samples. $\tau_1(d_r)$ in multilayers, apparently, does not obey any rule being more close to this value in the reference $TbCo_2$ film.

This means that not only r_d, but other factors come into play. This can be a different number of layers, which can also be responsible for an increase of Gilbert damping for the same sample. The Gilbert damping α shows a trend to increase with the r_d increase analogously to the anisotropy field dependence, but with a drop out of point B of the dependence (figure 4(b)). In magnetic multilayers, the presence of sharp interfaces causes a local increase of the interaction between spin waves and conduction electrons. This leads to an increase of the Gilbert spin-damping parameter near an interface [35]. In all multilayers studied here, the value of Gilbert damping is about an order of magnitude higher than in both $TbCo_2$ and FeCo single layers. Such an increase is typical for multilayers and can be measured with classical FMR [2, 35, 36] or optical pump-probe experiments [37, 38]. For low-excitation case, the main sources of the damping constant increase are: inhomogeneity and defects at the interfaces, spin transport and dephasing of spin waves through the interfaces. For high-excitation case, when hot electrons are generated by optical pulse, one can expect additional contribution from increased incoherency of spin transport and spin scattering at the interfaces.
Comparison of the experimental data with the results of calculations shows that the amplitudes of the anisotropy disruption A_1 and A_2 differ and decrease with an increase of the ratio r_d. This corresponds to the highest sensitivity of the monolayer FeCo to the optical pumping. The slow thermal relaxation of the anisotropy decelerates when the ratio r_d increases. It is worth emphasizing the correlation between amplitudes $A_{1,2}$ and anisotropy: the higher the anisotropy, the smaller the amplitudes. In other words, the stronger the anisotropy, the less it is suppressed.
In spin dynamics processes, impulse demagnetization δm(t) and suppression of the anisotropy δHA(t) participate jointly in the excitation of magnetization precession. In the geometry under consideration, the excitation is carried out by the y-component of the torque, in which demagnetization and anisotropy disruption enter additively as follows:

$$T_y = [\delta H_A + \delta m\,(4\pi + H_A/M)]\, M_x M_z / M. \quad (4)$$

Thus, we have to explain our choice in favor of the anisotropy. In our previous work we studied the spin dynamics in a similar structure but in the 'hard axis' configuration and magnetic field lying in the sample plane [30]. In this configuration within the LLG approach, demagnetization does not participate in the precession excitation. This way, the whole spin dynamics are described only in terms of the anisotropy suppression.
Additionally, in the hard axis configuration, magnetic field induced SRT occurs within the range of external magnetic field $-H_A < H < H_A$. In this SRT range, the direction of magnetization is determined by the competition between the magnetic field and the anisotropy field. In this case, the pulsed disruption of anisotropy deflects the in-plane magnetization in the direction of the field. This makes it possible to probe spin dynamics for different mutual orientations of magnetization and magnetic field by changing only the magnetic field.
Thus, our complete studies in configurations of 'easy axis' and 'hard axis' and conditions of rotation of magnetization within the SRT range allow us to describe spin dynamics in uniaxial intermetallic heterostructures within a unified approach of disruption of magnetic anisotropy.

4. Conclusions

Application of the optical pump-probe technique for studying ultrafast spin dynamics made it possible to obtain some general conclusions on the behavior and parameters of spin relaxation in $TbCo_2$/FeCo multilayers of various structure. The main role of magnetic anisotropy disruption in the optical excitation of the spin system is confirmed by comparison of the experimental results with modeling. In particular, the stronger the anisotropy, the less it is suppressed, that does not hold for magnetization. The anisotropy relaxation passes in three steps. The ultrafast one, caused by the spin-electron-phonon thermalization, occurs in τ_{th} = 2 ps. The further time range can be divided into two subranges: of τ_1 = 100 ps when the system is still hot and of further few nanoseconds when the system almost completely cools down. The

maximum amplitude of the photoinduced disruption of the anisotropy field $A_{th} + A_1 + A_2$ is about 14% for the pumping fluence of 7 mJ.cm^{-2}. The experimentally estimated spin precession frequency is about 20 GHz for the maximum value of the external field used in the experiment. The Gilbert damping in the multilayers is one order of magnitude higher than that in the constituent layers. The obtained results can serve as reference data in the development of spintronic devices based on $TbCo_2$/FeCo nanostructures.

Data availability statement

The data that support the findings of this study are available upon reasonable request from the authors.

Acknowledgments

This work was supported by Russian Science Foundation (Grant No. 20-12-00276). Fabrication of the samples was supported by French RENATECH network. The research was done using equipment of the Joint Core Facilities Center RTU MIREA.

Appendix. Experimental data processing

A typical photoinduced signal ΔS(t), obtained during the experiment at two opposite directions of the external magnetic field +H and −H, is shown in figure A1(a). The oscillating photoinduced polarization rotation ΔS(t) is observed against the background of exponential decay, which we associated with thermal contribution because the magnitude of it does not depend on the field H [39].

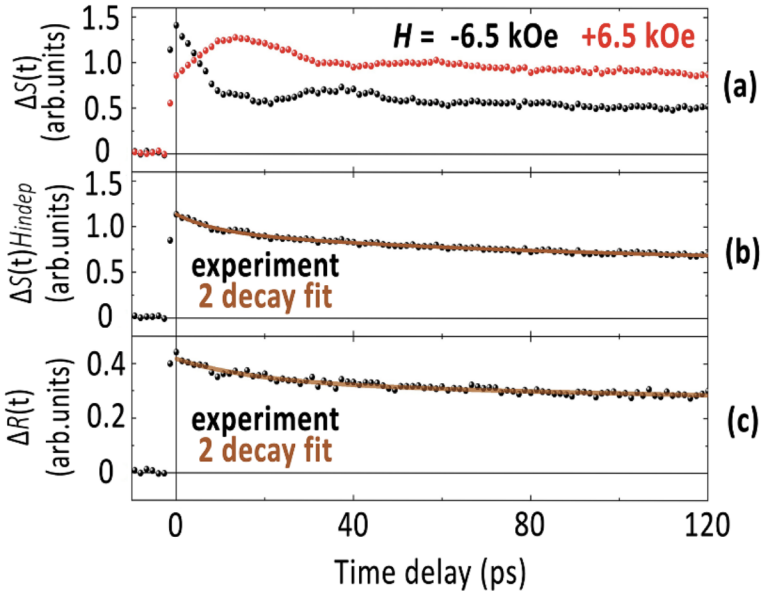

Figure A1. (a) Experimental photoinduced polarization rotation ΔS(t) at a magnetic field H of +6.5 and −6.5 kOe; (b) An isolated mean signal independent on the magnetic field and its two-decay fit; (c) Experimental photoinduced intensity of the reflected probe beam ΔR(t) and its two-decay fit.

Due to the symmetry of the experimental setup, Mz(+H) = −Mz(−H) and −Mx(+H) = Mx(−H), it is possible to exclude contribution to ΔS(t) that do not depend on the magnetic field. In order to use in the analysis only the signal depending on the magnetization, the signal difference was obtained for 2 orthogonal directions of the field [14, 28]. So, the Kerr rotation due to the dynamics of the magnetization vector is determined as

$$\Delta\theta_K(t,H) = \Delta S(t,H) - \Delta S(t)_{Hindep}, \quad (A.1)$$

where $\Delta S(t)_{Hindep}$ — contribution in $\Delta\Theta_K(t, H)$, independent on amplitude and direction of external magnetic field H. It was obtained as:

$$\Delta S(t)_{Hindep} = \left(\frac{\Delta S(t,+H) + \Delta S(t,-H)}{2} \right) \tag{A.2}$$

This field-dependent part of photoinduced signal is the subject of modeling for all samples described in the article. It is also worth noting that the photoinduced background signal $\Delta S(t)_{Hindep}$ (figure A1(b)) was observed both in the photoinduced polarization rotation $\Delta S(t)$ (figure A1(a)) and in the photoinduced reflection coefficient dynamics $\Delta R(t)$ (figure A1(c)). These dependences were fitted by a two-exponential dependence, the first time for each of the curves was tens of picoseconds, and the second time was hundreds of nanoseconds. The nature of these dependencies is beyond the scope of this article.

ORCID iDs
Sergei Ovcharenko https://orcid.org/0000-0002-6360-3672
Mikhail Gaponov https://orcid.org/0000-0003-0003-5054
Alexey Klimov https://orcid.org/0000-0002-5312-4061
Nicolas Tiercelin https://orcid.org/0000-0001-7400-4272
Philippe Pernod https://orcid.org/0000-0002-6708-8487
Elena Mishina https://orcid.org/0000-0003-0387-5016
Alexander Sigov https://orcid.org/0000-0002-1216-3339
Vladimir Preobrazhensky https://orcid.org/0000-0002-6206-5948

References

[1] Byun J, Kang D H and Shin M 2021 Switching performance comparison between conventional SOT and STT-SOT write schemes with effect of shape deformation AIP Adv. 11 015035
[2] Urban R, Woltersdorf G and Heinrich B 2001 Gilbert damping in single and multilayer ultrathin films: role of interfaces in nonlocal spin dynamics Phys. Rev. Lett. 87 217204
[3] Yu H et al 2015 Magnetic thin-film insulator with ultra-low spin wave damping for coherent nanomagnonics Sci. Rep. 4 6848
[4] Jamali M, Kwon J H, Seo S-M, Lee K-J and Yang H 2013 Spin wave nonreciprocity for logic device applications Sci. Rep. 3 3160
[5] Silva T J and Rippard W H 2008 Developments in nano-oscillators based upon spin-transfer point-contact devices J. Magn. Magn. Mater. 320 1260–71
[6] Haidar M, Awad A A, Dvornik M, Khymyn R, Houshang A and Åkerman J 2019 A single layer spin-orbit torque nano-oscillator Nat. Commun. 10 2362
[7] Hirohata A, Yamada K, Nakatani Y, Prejbeanu I-L, Diény B, Pirro P and Hillebrands B 2020 Review on spintronics: Principles and device applications J. Magn. Magn. Mater. 509 166711
[8] Kirilyuk A, Kimel A V and Rasing T 2010 Ultrafast optical manipulation of magnetic order Rev. Mod. Phys. 82 2731–84
[9] Lloyd-Hughes J et al 2021 The 2021 ultrafast spectroscopic probes of condensed matter roadmap J. Phys. Condens. Matter 33 353001
[10] Beaurepaire E, Merle J C, Daunois A and Bigot J Y 1996 Ultrafast spin dynamics in ferromagnetic nickel Phys. Rev.Lett. 76 4250–3
[11] Koopmans B, Malinowski G, Dalla Longa F, Steiauf D, Fähnle M, Roth T, Cinchetti M and Aeschlimann M 2010 Explaining the paradoxical diversity of ultrafast laser-induced demagnetization Nat. Mater. 9 259–65
[12] Baranov P G et al 2019 Spintronics of semiconductor, metallic, dielectric and hybrid structures (100th anniversary of the Ioffe Institute) Phys.-Usp. 62 795–822
[13] Wang C and Liu Y 2020 Ultrafast optical manipulation of magnetic order in ferromagnetic materials Nano Converg. 7 35
[14] Shelukhin L A, Pavlov V V, Usachev P A, Shamray P Y, Pisarev R V and Kalashnikova A M 2018 Ultrafast laser-induced changes of the magnetic anisotropy in a low-symmetry iron garnet film Phys. Rev. B 97 014422

[15] Ovcharenko S V, Gaponov M S, Ilyin N A, Logunov M V, Anhua W and Mishina E D 2020 Laser-induced spin dynamics in the iron-yttrium garnet film doped with Si ions Russ. Technol. J. 8 58–66
[16] Carpene E, Mancini E, Dallera C, Puppin E and De Silvestri S 2010 Three-dimensional magnetization evolution and the role of anisotropies in thin Fe/MgO films: Static and dynamic measurements J. Appl. Phys. 108 063919
[17] Khokhlov N E, Gerevenkov P I, Shelukhin L A, Azovtsev A V, Pertsev N A, Wang M, Rushforth A W, Scherbakov A V and Kalashnikova A M 2019 Optical excitation of propagating magnetostatic waves in an epitaxial galfenol film by ultrafast magnetic anisotropy change Phys. Rev. Appl. 12 044044
[18] Kimel A V and Li M 2019 Writing magnetic memory with ultrashort light pulses Nat. Rev. Mater. 4 189–200
[19] Wu Y, Elyasi M, Qiu X, Chen M, Liu Y, Ke L and Yang H 2017 High-performance THz emitters based on ferromagnetic/nonmagnetic heterostructures Adv. Mater. 29 1603031
[20] Khusyainov D et al 2021 Polarization control of THz emission using spin-reorientation transition in spintronic heterostructure Sci. Rep. 11 697
[21] Preobrazhensky V, Klimov A, Tiercelin N, Dusch Y, Giordano S, Churbanov A, Mathurin T, Pernod P and Sigov A 2018 Dynamics of the stress-mediated magnetoelectric memory cell Nx(TbCo2/FeCo)/PMN-PT J. Magn. Magn. Mater. 459 66–70
[22] Le Gall H, Ben Youssef J, Socha F, Tiercelin N, Preobrazhensky V and Pernod P 2000 Low field anisotropic magnetostriction of single domain exchange-coupled (TbFe/Fe) multilayers J. Appl. Phys. 87 5783–5
[23] Gambino R J, Plaskett T S and Ruf R R 1988 Exchange coupled magneto-optic layers IEEE Trans. Magn.24 2557–9
[24] Quandt E and Ludwig A 1999 Giant magnetostrictive multilayers(invited) J. Appl. Phys. 85 6232–7
[25] Xu Y, Chen D, Tong S, Chen H, Qiu X, We i D and Zhao J 2020 Spin polarization compensation in ferrimagnetic Co1-xTbx/Pt bilayers revealed by spin Hall magnetoresistance Phys. Rev. Appl. 14 034064
[26] Heigl M, Mangkornkarn C, Ullrich A, Krupinski M and Albrecht M 2021 Enhanced annealing stability of ferrimagnetic Tb/FeCo multilayers AIP Adv. 11 085112
[27] Gaponov M, Ovcharenko S, Klimov A, Tiercelin N, Pernod P, Mishina E, Ilyin N, Sigov A and Preobrazhensky V 2020 Ultrafast magnetization dynamics in the vicinity of spin reorientation transition in TbCo2/FeCo heterostructures J. Phys. Condens. Matter 32 225803
[28] Choi G-M, Schleife A and Cahill D G 2017 Optical-helicity-driven magnetization dynamics in metallic ferromagnets Nat. Commun. 8 15085
[29] Bigot J-Y, Vomir M, Andrade L H F and Beaurepaire E 2005 Ultrafast magnetization dynamics in ferromagnetic cobalt: the role of the anisotropy Chem. Phys. 318 137–46
[30] Ovcharenko S, Gaponov M, Klimov A, Tiercelin N, Pernod P, Mishina E, Sigov A and Preobrazhensky V 2020 Photoinduced spin dynamics in a uniaxial intermetallic heterostructure TbCo2 /FeCo Sci. Rep. 10 15785
[31] Bezuglyi A I and Shklovskii V A 1997 The kinetics of low-temperature electron-phonon relaxation in a metallic film following instantaneous heating of the electrons J. Exp. Theor. Phys. 84 1149–63
[32] Wietstruk M et al 2011 Hot-electron-driven enhancement of spin-lattice coupling in Gd and Tb 4f ferromagnets observed by femtosecond x-ray magnetic circular dichroism Phys. Rev. Lett. 106 127401
[33] Roth T, Schellekens A J, Alebrand S, Schmitt O, Steil D, Koopmans B, Cinchetti M and Aeschlimann M 2012 Temperature dependence of laser-induced demagnetization in Ni: a key for identifying the underlying mechanism Phys. Rev. X 2 021006
[34] Gerevenkov P I, Kuntu D V, Filatov I A and L A Shelukhin, Wang M, Pattnaik D P, Rushforth A W, Kalashnikova A M and Khokhlov N E 2021 Effect of magnetic anisotropy relaxation on laser-induced magnetization precession in thin galfenol films Phys. Rev. Mater. 5 094407
[35] Berger L 2001 Effect of interfaces on Gilbert damping and ferromagnetic resonance linewidth in magnetic multilayers J. Appl. Phys. 90 4632–8
[36] Barati E and Cinal M 2017 Gilbert damping in binary magnetic multilayers Phys. Rev. B 95 134440
[37] Song H-S, Lee K-D, Sohn J-W, Yang S-H, Parkin S P, You C-Y and Shin S-C 2013 Relationship between Gilbert damping and magneto-crystalline anisotropy in a Ti-buffered Co/Ni multilayer system Appl. Phys. Lett. 103 022406

[38] Kimura T et al 2018 Spin transfer torque switching of Co/Pd multilayers and Gilbert damping of Co-based multilayers Jpn. J. Appl. Phys. 57 09TD01
[39] Stupakiewicz A, Chizhik A, Zhukov A, Ipatov M, Gonzalez J and Razdolski I 2020 Ultrafast magnetization dynamics in metallic amorphous ribbons with a giant magnetoimpedance response Phys. Rev. Appl. 13 044058